



**HAL**  
open science

## **In vivo estimation of normal left ventricular stiffness and contractility based on routine cine MR acquisition**

Gerardo Rumindo, Jacques Ohayon, Pierre Croisille, Patrick Clarysse

### ► **To cite this version:**

Gerardo Rumindo, Jacques Ohayon, Pierre Croisille, Patrick Clarysse. In vivo estimation of normal left ventricular stiffness and contractility based on routine cine MR acquisition. *Medical Engineering & Physics*, 2020, 85, pp.16-26. 10.1016/j.medengphy.2020.09.003 . hal-03093687v2

**HAL Id: hal-03093687**

**<https://hal.science/hal-03093687v2>**

Submitted on 30 Sep 2021

**HAL** is a multi-disciplinary open access archive for the deposit and dissemination of scientific research documents, whether they are published or not. The documents may come from teaching and research institutions in France or abroad, or from public or private research centers.

L'archive ouverte pluridisciplinaire **HAL**, est destinée au dépôt et à la diffusion de documents scientifiques de niveau recherche, publiés ou non, émanant des établissements d'enseignement et de recherche français ou étrangers, des laboratoires publics ou privés.

# In vivo estimation of normal left ventricular stiffness and contractility based on routine cine MR acquisition

Gerardo Kenny Rumindo<sup>a</sup>, Jacques Ohayon<sup>b</sup>, Pierre Croisille<sup>a</sup>, Patrick Clarysse<sup>a</sup>,

<sup>a</sup>Univ Lyon, INSA-Lyon, Université Claude Bernard Lyon 1, UJM-Saint Etienne, CNRS, Inserm, CREATIS UMR 5220, U1206, F69621, LYON, France

<sup>b</sup>University Savoie Mont-Blanc, Polytech Annecy-Chambéry and Laboratory TIMC-IMAG, UGA, CNRS UMR 5525, Grenoble, France.

---

## Abstract

Post-myocardial infarction remodeling process is known to alter the mechanical properties of the heart. Biomechanical parameters, such as tissue stiffness and contractility, would be useful for clinicians to better assess the severity of the diseased heart. However, these parameters are difficult to obtain in the current clinical practice. In this paper, we estimated subject-specific *in vivo* myocardial stiffness and contractility from 21 healthy volunteers, based on left ventricle models constructed from data acquired from routine cardiac MR acquisition only. The subject-specific biomechanical parameters were quantified using an inverse finite-element modelling approach. The personalized models were evaluated against relevant clinical metrics extracted from the MR data, such as circumferential strain, wall thickness and fractional thickening. We obtained the ranges of healthy biomechanical indices of  $1.60 \pm 0.22$  kPa for left ventricular stiffness and  $95.13 \pm 14.56$  kPa for left ventricular contractility. These reference normal values can be used for future model-based investigation on the stiffness and contractility of ischemic myocardium.

*Keywords:* left ventricle model, finite element analysis, cine MRI, myocardial stiffness, myocardial contractility, ischemic heart disease

---

## 1. Introduction

Ischemic heart disease occurs due to the constriction of the coronary arteries, causing reduced supply of blood and oxygen to the heart muscles. This eventually leads to myocardial functional impairment and scarring. Post-infarction remodeling modifies the mechanical behavior of the myocardium [1], making stiffness and contractility good potential prognostic parameters. Unfortunately, clinicians normally lack information on these biomechanical parameters, since direct measurement is very challenging, if not impossible. Mechanical models capable of predicting subject-specific stiffness and contractility would be a useful tool to assess the condition of an ischemic patient. However, before performing any measurement on ischemic hearts, it is necessary to first establish the range of normal LV stiffness and contractility.

The determination of subject-specific constitutive material parameters is a challenging inverse problem involving several key components: hearts shape, tissue structure and motion representation, myocardial material modeling, definition of appropriate boundary and loading conditions and optimization strategy [2]. Cardiac imaging modalities such as cardiac magnetic resonance (CMR) now provide access to several of the complementary information needed to build cardiac models e.g. geometry, tissue characteristics, and motion. Several finite element (FE)-based studies have addressed the identification of diastolic mechanical parameters of the myocardium within an optimization process in reference to myocardial displacement [3, 4], strains [5], strains and volumes either simultaneously [6] or separately [7, 8]. Estimation of myocardial contractility requires the incorporation of subject-specific active contraction, which often results in the estimation of one active parameter of various active tension formulations. Table 1 presents a non-exhaustive list of models (with initial geometry, active and passive constitutive laws, and boundary conditions used) developed to estimate the passive and active mechanical properties of the myocardium. The variety of estimated passive parameters in various conditions is visible in Table 4 for human studies. Genet et al. proposed a personalization method to construct a

reference left ventricular stress map [7]. Their study managed to find a normal range of myocardial contractility, but it was limited to five healthy subjects who underwent extensive CMR acquisitions, which are time-consuming, costly, and not suitable for every individual.

Table 1: Comparative table detailing recent modelling studies. H: healthy subject, P: pathological subject; HFpEF, HFrEF: Heart failure with preserved/reduced ejection fraction; ES: end-systole, ED: end-diastole, BD: Beginning diastole; ESP: end-systolic pressure, EDP: end-diastolic pressure; EDV: end-diastolic volume, EDS: end-systolic volume; FT: feature tracking; CMR: Cardiac Magnetic Resonance; NA: not applicable. FG: Fung-Guccione law [9]; HO: Holzapfel-Ogden law [10]; BSC: Bestel-Clement-Sorine model [11], Time-varying elastance model [12]; h, t: spatial helix/transverse angle distribution of the myocardial fibers.

Study	H: healthy P: pathological	Anatomical modeling			Constitutive law		Boundary conditions
		Reference geometry / modality	Fiber	Motion Modality / Quantification	Passive	Active	
Asner, et al., 2017 Asner, et al., 2016 [14-15]	1H, 2P 3H, 3P	LV at ES / CMR	h: linear t: NA	3D-tag & Cine CMR / displacement from IRTK Image registration Toolkit	Reduced HO law, 4 parameters	Time & length-dependent active tension parameter $\alpha(t)$	- Endocardial volumes and basal displacements - Cuff-measured ESP - EDP from mitral flow velocity
Balaban, et al., 2018 [43]	1P	LV at beginning of atrial systole / 4D-US	h: Rule-based [46]	4D-US / regional strains from GE's package EchoPac	Simplified HO law	NA	- Zero longitudinal displacement at the base, elastic in the other directions - LV cavity pressure measured through catheterization
Gao, et al., 2017 [6]	27H, 11P	LV at ED / CMR	h: linear t: linear	Cine-CMR / b-spline registration to estimate regional circumferential strain	HO law, 8 parameters	Active tension [48], Parameter $T_{req}$	- Imposed EDP: 8 mmHg (H), 16 mmHg (P) - Cuff-measured ESP - MI scar: 50 x stiffer
Genet, et al., 2014 [7]	5H	LV at BD / CMR	h: linear t: NA	Tagged-CMR / systolic regional strains from FindTags	FG law, 4 parameters	Time-varying elastance model Parameter $T_{max}$	- Fixed basal line - Prescribed volume changes EDV and ESV
Marchesseau, et al., 2013 [44]	8H, 3P	Biventricular / CMR	h: linear t: NA	Cine-CMR / Time Diffeomorphic FFD for endocardial surface points tracking	Isotropic visco- hyperelastic (Moonley & Rivlin), BSC model, 14 parameters	BSC model, 14 parameters	- Arterial pressure modeled by a 4 element Windkessel model
Nasopoulou et al., 2017 [27]	1H, 7P	LV at minimum pressure / CMR	h: linear t: NA	Cine-CMR / Non-rigid registration for displacement	FG law, $C_1$ and $\alpha = r_j + r_i + r_{jt}$	NA	- LV pressure measured through catheterization - Data-prescribed motion of the basal plane nodes
Rumindo et al. (This paper)	21H	LV at ES / CMR	h, t: Rule- based [16]	Cine-CMR / FT for ES circumferential strain	Simplified FG law, 2 parameters $C_0, b_j$	Time-varying elastance model Parameter $T_{max}$	- Fixed base, boundary-free epicardium, - Prescribed volume change
Walker, et al., 2005 [5]	5P-sheeps	LV at end isovolumic relaxation / CMR	h: linear t: NA	Tagged-CMR / ES strains from 4D B-spline method	FG law	Time-varying elastance model Parameter $T_{max}$	- Azimuthal displacements constrained at all nodes at the base and apex. - ESP and EDP measured through catheterization
Wang, et al., 2016 [45]	2 WKY, 2 SHR rats	LV at BD / CMR	h: linear Homogenous sheet angle=30°	LV chamber compliance from pressure-volume curves	Modified HO law, 8 parameters	NA	- Imposed intracavity pressure from 0 to 15 mmHg - LV chamber compliance as optimization metrics
Wang, et al., 2018 [28]	5H, 11 HFpEF, 8 HFrEF	LV at diastasis / CMR	Math. Model [47]	Cine-CMR / LV best surfaces fit	FG law, 4 parameters (only c1 personalized)	NA	- Catheter measurements of LV, aortic and pulmonary pressures
Xi, et al., 2013 Xi, et al., 2014 [3, 40]	1H, 2P	LV at BD / CMR	h: linear t: NA	3D-tag & Cine CMR / meshes matching from IRTK Image registration Toolkit	Reformulated FG law, 4 parameters: $c_1, \alpha, r_3, r_4$	Length-dependent active term (early-diastole) [49], Parameter $T_2$	- Prescribed displacement at base plane and apex - LV pressure measured through catheterization

In this study, we aim to estimate left ventricular stiffness and contractility of 21 healthy subjects based on routine cardiac cine CMR acquisition. These biomechanical parameters are quantified by personalizing a FE mechanical model of the LV. The models were validated individually through comparison against measured strains and other clinically relevant measurements, i.e. end-diastolic wall thickness, systolic fractional thickening, global circumferential and longitudinal strains. The main goal of this study is to propose an initial step toward estimating and verifying subject-specific left ventricular stiffness and contractility based on routine CMR acquisitions.

## 2. Methods

### *Subjects datasets*

Two cardiac MR datasets of healthy volunteers were used in this study. The first dataset (n=11, 9 males) is open-access, available within the context of a MICCAI STACOM Challenge [13]. The second dataset was part of the MARVEL cohort run by CHU Saint-Etienne, France (n=10, 4 males). The MARVEL study (ID RCB 2016-A00913-48) was approved by the local ethical committee (URB #6/052) and is registered at ClinicalTrials.gov (NCT03064503). All patients provided written informed consent. Unfortunately, no pressure measurements were recorded during the examinations for these two datasets.

### *Processing of MR data*

The MICCAI dataset has a pixel size of 1.25 mm and a slice thickness of 8 mm, whereas the MARVEL dataset has a pixel size of 0.55 mm and a slice thickness of 7 mm. LV segmentation was performed on the short-axis, the 2-chamber and 4-chamber long-axis images within CVI42 software (©Circle Cardiovascular Imaging Inc., Figure 1-top). The end-systolic (ES) and end-diastolic (ED) volumes of each subject were computed from the segmented endocardial surfaces. The LV wall was meshed with hexahedral elements in the FE software ABAQUS (©Dassault Systemes) (Figure 2). The mesh for each model consisted of  $3745 \pm 450$  C3D8R elements and  $4521 \pm 539$  vertices. We verified our

chosen mesh density via a mesh convergence analysis. The ES strains for each subject were computed using the Feature Tracking (FT) technique available in CVI42 (Figure 1-bottom). The ES strain was calculated with respect to ED configuration.

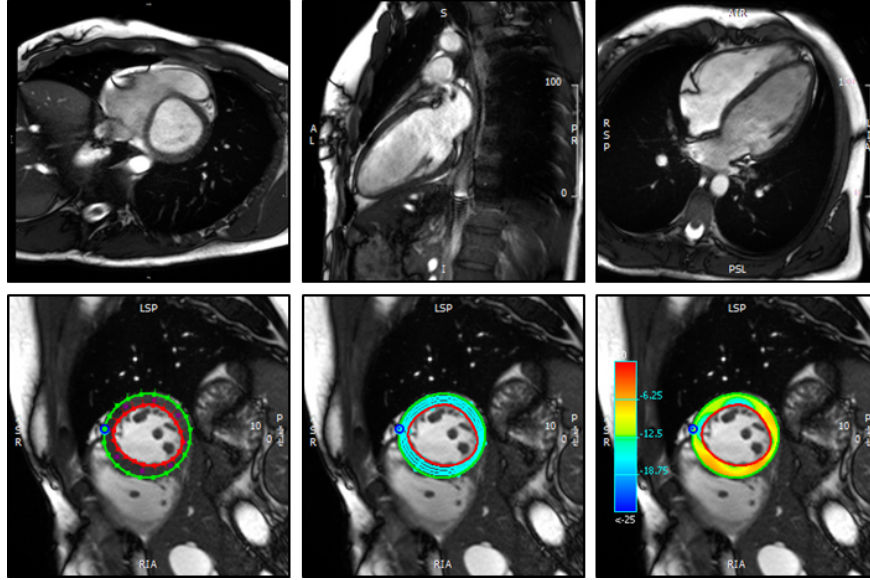


Figure 1: Top: short-axis, 2-chamber and 4-chamber long-axis *cine* images (from left to right). Bottom: Feature Tracking results; boundary points, tracking mesh, circumferential strain map (from left to right)

### *LV myocardial modelling*

In the present work, the ES geometry has been chosen as the reference configuration ; it was directly accessible from clinical MRI data (with the end-diastolic one). We therefore assumed that the ES geometry was closer to the one at the end of isovolumic relaxation configuration [14, 15], the state where both volume and pressure are minimal and the closest to unloaded configuration. Figure 3 illustrates the fiber arrangement attributed to the LV myocardium according to the description in [16]. Appendix A provides the mathematical formulation of the myocardial fiber arrangement.

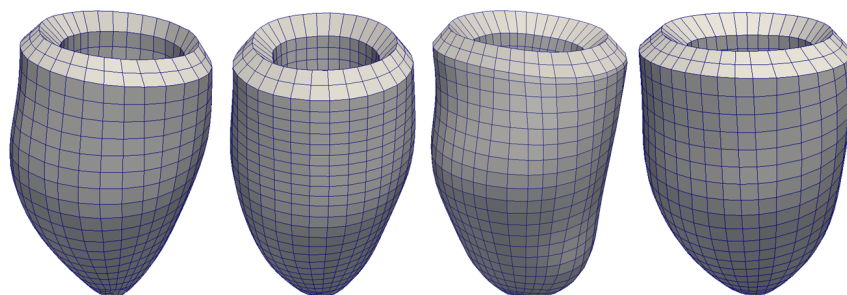


Figure 2: Meshed geometries of the left ventricles at end systole from four subjects

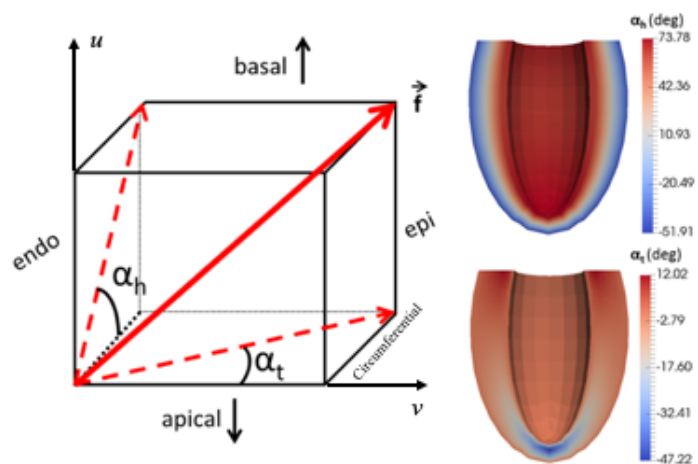


Figure 3: Left: definition of helix ( $\alpha_h$ ) and transverse ( $\alpha_t$ ) angles within the normalized coordinate system (Appendix A). Right: spatial distribution of helix angle (top) and transverse angle (bottom)

Myocardial passive behavior was modeled by transversely-isotropic hyper-elastic material [9], while active behavior was defined by a stretch-dependent active law [12]. They were implemented in the user material (UMAT) subroutine for the FE solver ABAQUS/Standard.

The passive material behavior is parameterized by 4 material parameters ( $C_0, b_f, b_t, b_{ft}$ ).  $C_0$  is the linear constant that determines the overall isotropic stiffness of the myocardium,  $b_f, b_t$  determines the stiffness in the local myocardial fiber directions, and the transverse directions, respectively, whereas  $b_{ft}$  defines the shear stiffness. The ratio of  $b_f$  to  $b_t$  to  $b_{ft}$  was kept fixed at 1.0 to 0.4 to 0.7, in accordance to the finding of Wenk et al. [17]:  $b_t = 0.4b_f$ ;  $b_{ft} = 0.7b_f$ . This approach limits the material parameters identification to 2 parameters,  $C_0$  and  $b_f$ . The active stress law is linearly-scaled by its maximal value  $T_{max}$ , which needs to be identified for each subject. Further details can be found in Appendix B.

The base ring was kept fixed (Figure 2), while the epicardium was boundary-free. In the normal heart, the base plane exhibits a large longitudinal displacement toward the apex (up to 1cm) while the apex moves much less. However, the imposed constraint (adopted in most of the 3D finite element simulations) helps to stabilize the numerical solution and should not drastically alter the intraparietal distributions of stresses and strains, which are the mechanical responses of interest in this study. FE Simulations were performed by imposing a prescribed volume change to the LV cavity using an integrated optimization process available in the ABAQUS software, which iteratively calculates the amplitude of the cavity pressure that must be imposed in order to satisfy the required LV volume. Quasi-incompressibility is enforced by setting the bulk modulus to be close to that of water [18].

#### *Model personalization*

Three parameters were to be identified for each subject;  $C_0$  and  $b_f$  for the passive law, and  $T_{max}$  for the active law. We identified the passive and active parameters separately using a 2-point simulation approach [7, 19].

The passive parameters  $C_0$  and  $b_f$  were identified so that the distance between the simulated end-diastolic pressure-volume relationship (EDPVR) and that of Klotz et al. [20] was minimized. Note that the value of the ED pressure results from this optimization process (close to  $9mmHg = 1.2kPa$ ). Once the passive parameters  $C_0$  and  $b_f$  were identified for each subject, the active parameter  $T_{max}$  was identified by matching a normal ES pressure of  $120mmHg(16kPa)$ .

The parameters identification was performed using the Nelder-Mead optimization available in MATLAB (©MathWorks) [21]. The cost function for the diastolic personalization was the sum of squared error between the "Klotz" curve pressure  $P_{klotz}$  and the predicted pressure  $P_{sim}$  for the corresponding normalized volume values  $i$  being compared. For the systolic personalization, the active material parameter was optimized to result in the targeted ES pressure.

#### *Model evaluation*

*In vivo* ES circumferential strain values measured with FT technique on *cine* MR images were interpolated on the finite-element mesh. These interpolated strains were compared with the personalized simulation strains. Only circumferential strains were compared, as radial strain extracted from FT technique was found to not correlate well with other LV strain measurement techniques [22, 23], and to be less robust and reproducible [24, 25]. Longitudinal strains were not compared as only 2-long-axis images were acquired, leading to insufficient number of calculated strain points for our validation purpose.

A set of global LV function metrics were calculated from the subject-specific models: ED wall thickness ( $EDWT$ ), systolic fractional thickening ( $SFT$ ), global longitudinal strain ( $GLS$ ) and segmental rotations ( $ROT$ ). These LV metrics were obtained referring to Figure 4 as follows:

- **EDWT**: wall thickness at ED (mm)
- **SFT** =  $100 * (ESWT - EDWT) / EDWT$ : systolic fractional thickening (%), i.e. the relative difference between the wall thickness at ES and ED with respect to ED

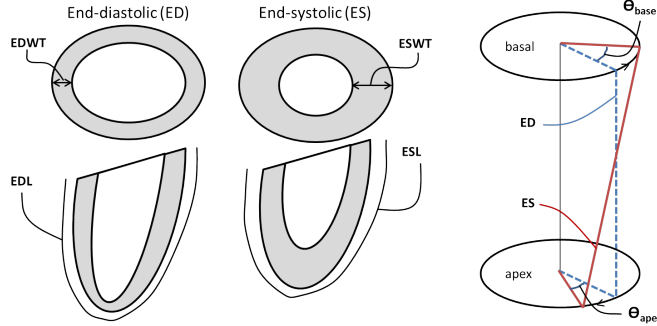


Figure 4: Illustration for the LV metrics. See text for the complete formula (EDWT and ESWT: end-diastolic and end-systolic wall thickness, EDL and ESL: end-diastolic and end-systolic length,  $\theta_{base}$  and  $\theta_{apex}$ : basal and apical rotations)

- **GLS** =  $100 * (EDL - ESL)/EDL$ : global longitudinal strain (%), the relative difference between the length along the myocardial longitudinal direction at ES and ED with respect to ED.
- **ROT<sub>base</sub>** and **ROT<sub>apex</sub>**: segmental rotation (degrees), which are calculated by observing the angular displacement of a point at basal and apical levels with respect to the LV axis, denoted as  $\theta_{base}$  and  $\theta_{apex}$  in Figure 4, respectively. We assumed counter-clockwise rotation to be positive as seen from apex.

As an additional method evaluation, the metrics obtained from the midventricle region of the personalized models were compared to the ones measured from *cine* MR images and to the normal values found in literatures. The model-predicted *EDWT* and *SFT* values were compared to the values computed from the MR images. Moreover, all four metrics from our personalized models were also compared to the normal values found in literature.

#### *LV stiffness and contractility indices*

We use the initial Young's modulus of the passive myocardium in the fiber direction to represent the subject-specific LV stiffness with one scalar index.

The mathematical expression of this parameter is detailed in Appendix B. This stiffness index (**SI**) reflects the behavior of the transversely isotropic incompressible passive myocardium at its initial configuration (i.e. zero-stress state). We considered the optimized  $T_{max}$  parameter as the subject-specific index of myocardial contractility (**CI**). Both indices are expressed in kPa.

Table 2: Mean and standard deviation (SD) of LV metrics across all subjects, as well as the differences between measured and personalized simulated values (Ecc: circumferential strain, GLS: global longitudinal strain).

Subject metrics n = 21, 13 male		Measured (meas)	Simulated (sim)	meas-sim
Volume (ml)	End-diastole	137.3 (25.8)		-
	End-systole	58.8 (11.6)		
Pressure (kPa)	End-diastole	1.2 (prescribed)	1.28 (0,0014)	0.08 (0,0014)
	End-systole	16		-
Ejection fraction (%)		57.1 (3.7)		-
ED wall thickness (mm)		7.3 (1.5)	7.9 (1.6)	-0.56 (0.98)
Systolic fractional thickening (%)		67.4 (23.7)	69.2 (8.5)	-1.8 (24.4)
$E_{cc}$ (%)		-17.4 (2.6)	-17.0 (2.6)	-0.89 (3.8)
GLS (%)		-9.8 (3.7)	-15.1 (1.9)	5.3 (4.3)

### Statistical analysis

The correlations between the ejection fraction (EF), myocardial volume, end-diastolic or end-systolic volume, contraction index (**CI**) and stiffness index (**SI**) were analyzed by multiple linear regression using a commercially available software package (SigmaStat 3.5, Systat Software, Inc., Point Richmond, CA, USA). Regressions with probability values  $p < 0.001$  were considered statistically significant.

### 3. Results

#### *Subject-specific MR data*

Table 2 displays the LV metrics for all subjects. 'Measured' lists the metrics obtained from the MR data. ED wall thickness is established to be different between male and female: in our study we found ED wall thickness of  $8.1 \pm 1.3$  mm and  $6.1 \pm 0.8$  mm for male and female subjects, respectively.

Table 3: Subject-specific stiffness (*SI*) and contractility (*CI*) indices for the 21 subjects. The unit of the indices are in *kPa*

	#1	#2	#3	#4	#5	#6	#7	#8	#9	#10	#11
<i>SI</i>	1.61	1.46	1.69	1.63	1.73	1.97	1.24	1.56	1.46	1.67	1.38
<i>CI</i>	92.92	82.58	82.66	79.79	89.40	97.16	78.29	81.19	86.86	84.20	124.83
	#12	#13	#14	#15	#16	#17	#18	#19	#20	#21	Mean(SD)
<i>SI</i>	1.50	1.56	1.56	1.81	1.84	1.56	1.92	1.01	1.62	1.75	1.60(0.22)
<i>CI</i>	98.41	100.42	88.22	115.61	115.76	99.71	109.27	87.95	121.47	80.95	95.13(14.56)

#### *Model personalization evaluation*

The one-parameter (*CI*) personalization process conducted to the targeted ES pressure of  $16kPa$  for all the cases. The average optimized ED pressure in the *SI* identification process was  $1.28kPa$ . Figure 5 shows an example of the personalized LV dynamics of a healthy volunteer, where the top figures show the distribution of ES myofiber strain and stress, and the bottom figures shows a midventricular slice of deformed simulated LV geometry at ED and ES superimposed with the respective MR images. The comparison of anatomical and functional parameters given in Table 2 also reports on the goodness-of-fit between imaging data and model i.e. ED wall thickness, systolic fractional thickening and circumferential strain for the short axis direction and the global longitudinal strain for the long-axis direction. Figure 6 shows the Bland-Altman

Table 4: Estimated constitutive law parameters for healthy cases from similar studies in the literature. **SI** and **CI** are our proposed stiffness and contractility indices, respectively.  $E^f$  and  $E^{cf}$  are the initial Young’s modulus in the fiber and cross-fiber direction, respectively. (see Appendix B for details). The parameter  $\alpha$  is defined as

$$\alpha = b_f + b_t + b_{ft}.$$

Study	$C_0$ (kPa)	$b_f$	$b_t$	$b_{ft}$	$\alpha$	<b>SI</b> = $E^f$ (kPa)	$E^{cf}$ (kPa)	$E^f/E^{cf}$	<b>CI</b> (kPa)
Our study: mean	0.08	16.15	6.46	11.31	33.91	1.60	0.91	1.75	95.13
SD	$\pm 0.016$	$\pm 3.66$	$\pm 1.46$	$\pm 2.56$	$\pm 7.69$	$\pm 0.22$	$\pm 0.13$	-	$\pm 14.56$
Genet et al.[7]	0.12	14.40	5.76	10.08	30.24	1.99	1.14	1.75	143.00
Xi et al.[26]	0.30	41.71	9.07	51.52	102.30	13.87	4.96	2.80	NA
Xi et al.[3]	2.00	19.13	10.67	12.76	42.56	48.93	35.04	1.40	NA
Nasopoulou et al.[27]	1.70	8.00	3.00	4.00	15.00	16.15	8.81	1.83	NA
Wang et al.[28]	1.20	8.61	3.67	25.77	38.05	12.53	7.49	1.67	NA
Range	[0.08-2]	[8-41.71]	[3-10.67]	[4-51.52]	[15-102.3]	[1.60-48.93]	[0.89-35.04]	[1.4-2.8]	

plots comparing the measured and simulated ES circumferential strains, mid-ventricular ED wall thickness and systolic fractional thickening. Figure 7 shows the segmental circumferential strain error of our personalized models from the midventricular slices of four cases.

On average, our personalized models had an ED wall thickness of  $8.7 \pm 0.9$  mm (basal),  $8.9 \pm 0.7$  mm (medial),  $8.8 \pm 0.9$  mm (apical) for male subjects, and  $6.7 \pm 0.5$  mm (basal),  $6.3 \pm 1.0$  mm (medial),  $5.7 \pm 0.8$  mm (apical) for female subjects (Figure 8). Similarly, we divided the results from LV systolic fractional thickening into basal, medial and apical positions on the left ventricles (Figure 9(a)). On average, our personalized models resulted in SFT of  $72.0 \pm 17.7$  % (basal),  $69.2 \pm 8.5$  % (medial) and  $56.9 \pm 7.6$  % (apical). In addition, our personalized models lead to an average GLS values of  $-15.1 \pm 1.9$  % (Figure 9(b)). With respect to the ED condition, average segmental rotations of  $+11.8^\circ \pm$

$0.7^\circ$  and  $-3.0^\circ \pm 2.6^\circ$  for basal and apical levels, respectively, were observed in our models.

#### *Subject-specific biomechanical indices*

Table 3 lists the personalized material parameters and indices. The average LV stiffness index **SI** was  $1.60 \pm 0.22$  kPa across all subjects, while the average contractility index **CI** was  $95.13 \pm 14.56$  kPa. Those values are compared to values obtained by similar studies in Table 4. Multiple linear regression analyses were carried out on the 21 cases to look for potential correlations between the five following parameters: stiffness index (**SI**, unit: kPa), ejection fraction (**EF**), end-diastolic volume (**EDV**, unit: ml) or end-systolic volume (**ESV**, unit: ml), myocardial volume (**MV**, unit: ml), and the contractility index (**CI**, unit: kPa). Only two independent variables (namely, **SI** and **CI**) appear to be statistically correlated to **EF** estimation. We found that the ejection fraction increases with **CI** and decreases with **SI**:  $EF = 0.133CI - 19.782SI + 70.765$ , with  $R^2 = 0.96$  and  $p < 0.001$ . This shows a relationship between **SI**, **CI** and **EF** although the very small range of **EF** values ( $57.1 \pm 3.7\%$ ) for this population of normal subjects. It is expected that **SI** and **CI** would be able to differentiate subjects with reduced **EF** from controls and even subjects with preserved **EF** as nicely shown in [28].

#### **4. Discussion**

Despite the clear advantages for clinicians and biomedical engineers in estimating the *in vivo* left ventricular mechanical properties, no studies on a non-invasive estimation method have been developed and validated solely based on data acquired from routine clinical data. The present work is one of the first that use inverse FE modeling and measurements from routine cine CMR acquisitions to estimate subject-specific left ventricular stiffness and contractility on twenty-one healthy subjects. Our personalization approach was extensively evaluated against measured regional LV metrics in the form of circumferential

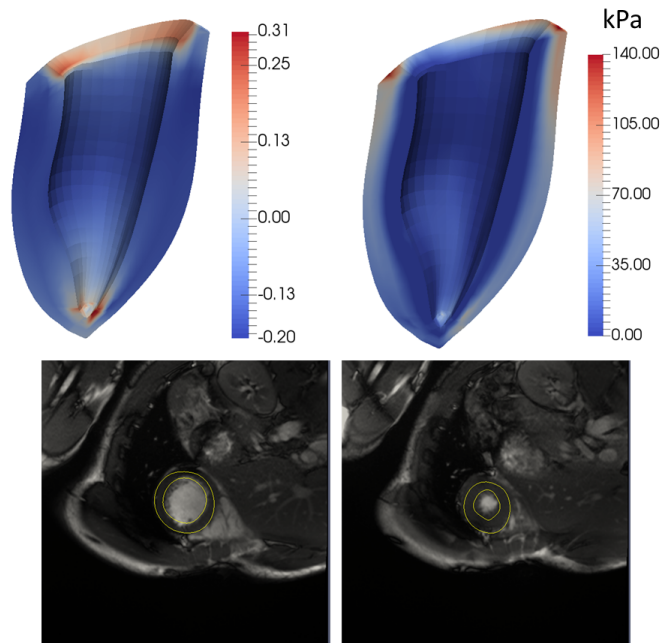
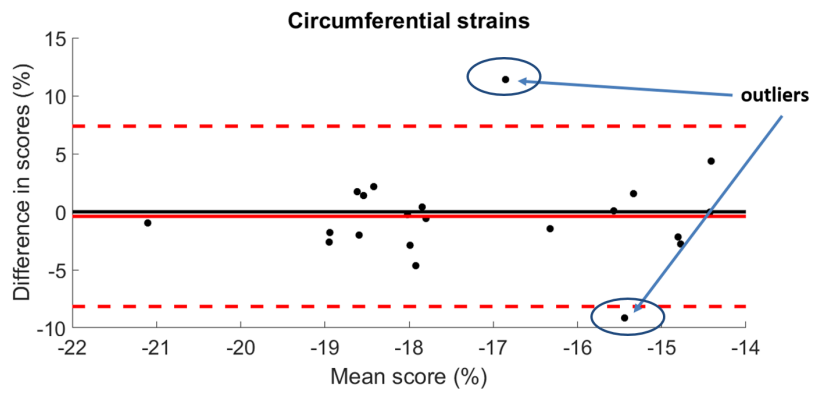
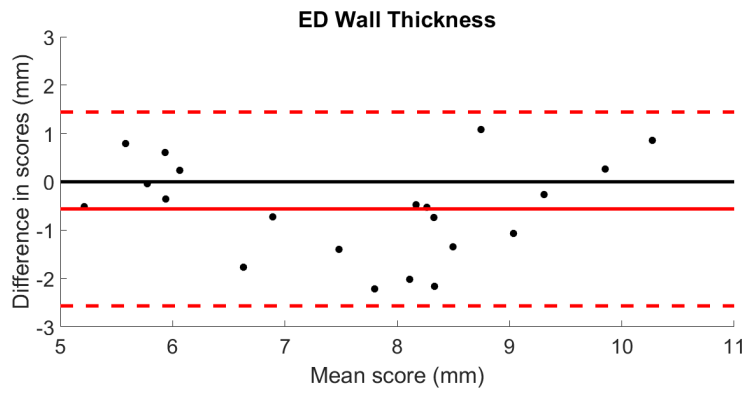


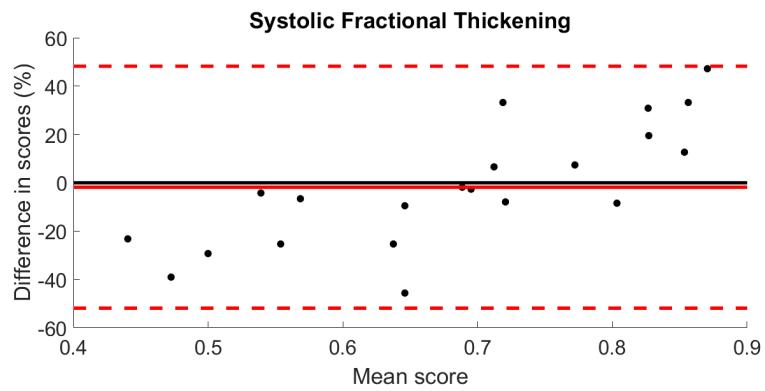
Figure 5: Personalized model from one healthy volunteer data (subject #5). Top: myofiber strain (left) and stress (right) at ES. Bottom: deformed midventricular slice of one LV model in yellow superimposed with the MR images at ED (left) and ES (right)



(a)



(b)



(c)

Figure 6: Bland-Altman plots: simulated vs MRI-based measurements for (a) circumferential strain (arrows indicate the outliers), (b) end-diastolic wall thickness, and (c) systolic fractional thickening.

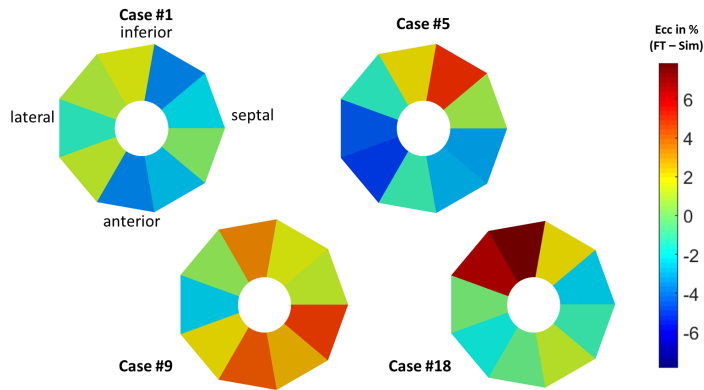


Figure 7: Segmental circumferential strain error (FT - personalized simulation) from a midventricular slice of four cases. The error is represented as a mean of circumferential strain point-to-point difference (simple subtraction) in each segment

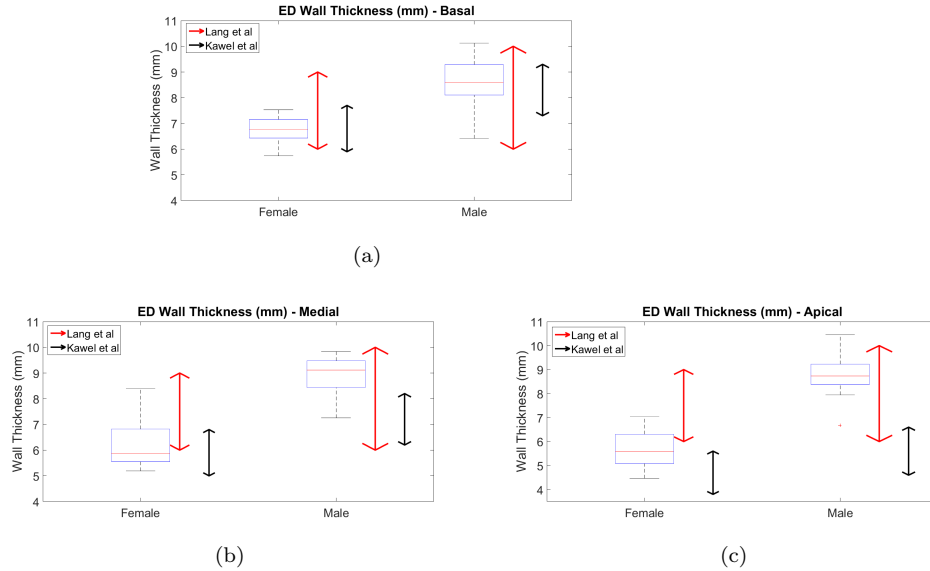


Figure 8: ED wall thickness calculated from the personalized models at basal (a), medial (b) and apical (c) levels for 21 subjects (13 males). The arrows are reference values from Lang et al. [29] (red) and Kawel et al. [30] (black)

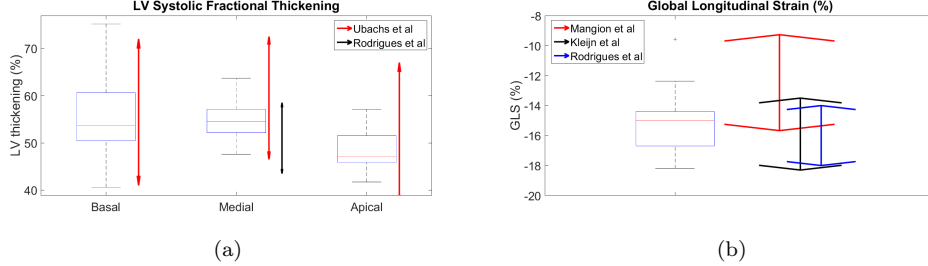


Figure 9: (a) LV thickening calculated from the personalized models at basal, medial and apical levels for 21 subjects. The arrows are reference values from Ubachs et al. [31] (red) and Rodrigues et al. [32] (black). (b) global longitudinal strain calculated from the personalized models for 21 subjects. The arrows are reference values from Mangion et al. [33] (red), Kleijn et al. [34] (black) and Rodrigues et al. [32] (blue)

strain values and against measured global LV metrics such as ED wall thickness and systolic fractional thickening. The range of biomechanical indices found in this study (Table 3) could serve as a reference for *in silico* diagnosis of potential cardiac pathologies. Table 4 presents the results of the estimation of mechanical parameters performed on the 21 healthy volunteers, with a comparison with some values reported in the literature. Because of the large variability observed in the values of the constitutive parameters, it remains difficult to compare them among the published works. This is notably due to the wide variety of approaches used to solve the inverse biomechanical problem. In addition, the obtained parameter values strongly depend on the optimization scheme used, the solution of which is generally not unique [26]. The lack of a standardized characterization of the passive properties of the myocardium (through e.g. 'normal' parameter value range) represents a major problem that limits the use of such patient-specific biomechanical modeling approaches for clinical diagnosis. One group has recently suggested that by simultaneously considering two cost functions, one based on energy and the other on geometry, it was possible to uniquely determine the set of solutions ( $C_0, \alpha = b_f + b_t + b_{ft}$ ) in the case of the constitutive law of the transversely isotropic material [27]. This is a promising

way to unify and compare stiffness measurements obtained by different authors and to extract clinically meaningful reference values. In a sensitivity study (not reported in this paper), the impacts of  $C_0$ ,  $b_f$ ,  $\mathbf{CI}$ , myofiber helix angle  $\alpha_h$ , and transverse angle  $\alpha_t$  onto myocardial mechanical strains ( $E_{cc}$ ,  $E_{rr}$ ,  $E_{ll}$ , and  $E_{rc}$ ) has been assessed at basal, mid and apical levels. Their values were varied between 0.7 and 1.3 times the reference value. It was observed that the evolution of the strains was globally consistent and smooth. In particular, both stiffness indices ( $C_0$  and  $b_f$ ), and therefore  $\mathbf{SI}$ , had a negative correlation with strains.  $\mathbf{CI}$  had a positive correlation with the radial strain  $E_{rr}$ .

The circumferential strains obtained with the FT technique were within the normal range as found in literature [30, 29, 32, 25, 31]. In total,  $771 \pm 132$  strain points were computed via the FT technique on cine MR images per subject for circumferential strain. The shift between measured and simulated values are in average low for ED wall thickness ( $-0.56 \pm 0.98mm$ ), systolic fractional thickening ( $-1.8 \pm 24.4\%$ ) and circumferential strain ( $-0.89 \pm 3.8\%$ ), indicating a good match in the radial-circumferential directions (Table 2). The average shift for GLS is however larger ( $5.3 \pm 4.3\%$ ). The average measured value is significantly high  $-9.8 \pm 3.7\%$ , and far from the range for normal human values [35, 36]. This probably results from the estimation that was based only on 2 long-axis images, which led to  $29 \pm 7$  longitudinal strain points computed on average per subject. On the contrary, the average simulated GLS value is closer to the normal range ( $-15.1 \pm 2\%$ ).

We also compared the global LV pump functions from the personalized models with the normal values found in literature. Figure 8 and Figure 9 show these comparisons for ED wall thickness, systolic fractional thickening and global longitudinal strain. The box-plots represent the values from our personalized model and the arrows represent the reference values found in literature. These LV metrics obtained from the MR data were also in agreement with literature.

The segmental rotations predicted by our personalized models were in agreement with [37, 38]. Since LV torsion is highly dependent on endocardial and epicardial contraction, LV geometry and myocardial fiber arrangement, this

showed that the rule-based myocardial fiber architecture in our model was able to produce realistic physiological torsional deformation of the LV.

No significant bias is observed for both ES circumferential strain and systolic fractional thickening. The bias for ED wall thickness is about  $-0.5\text{mm}$  expressing a slight tendency to higher MRI-based measurements (Figure 6(b)). There seems to have a magnitude dependence of the systolic fractional thickening (Figure 6(c)); this is not the case for the other measurements. While limits of agreement remain acceptable for circumferential strain and wall thickness (Figures 6(a) and 6(b)), they are significantly high for systolic fractional thickening (Figure 6(c)). Our personalized approach was able to produce similar circumferential strains to the measured ones (Figure 6(a)). However, two of the male subjects - #11 and #19 - were found to be outliers (Figure 6(a)). Table 5 lists in details the image-based measured ED wall thickness of these subjects, which were relatively thicker in comparison with the remaining male subjects and from the literature [30]. Furthermore, subject #11 had a reduced global circumferential strain of  $-11.2 \pm 6.7\%$  as measured with the FT technique, which might be an indication of hypertensive cardiomyopathy [39].

Table 5: MR-based ED wall thickness and circumferential strains of subjects #11 and #19 compared with the remaining 11 male subjects and literature values [30]

( $E_{cc}$ : circumferential strain)

Measurements Mean (SD)	ED wall thickness (mm)				$E_{cc}$ (%)
	basal	medial	apical	mean	
#11	10.8	8.0	8.5	9.1	-11.2 (6.7)
#19	8.8	9.2	6.7	8.2	-20.0 (7.2)
Others (n=11)	8.5 (1.1)	8.1 (1.3)	6.8 (1.2)	7.8 (1.0)	-17.6 (2.4)
Kawel et al. [30] (n=300)	8.3 (1.0)	7.2 (1.0)	5.6 (1.0)	7.03 (1.0)	-

The limitations of the present study are mainly related to modelling assumptions. The exclusion of the right ventricle in the model definitely affects the distribution of the circumferential strains. We also neglected the multi-physics aspects of a functional heart, i.e. hemodynamics and electrophysiology.

Another limitation is that, due to the absence of pressure measurements, our model personalization was based on normal ED and ES pressures found in literature. A very interesting study has considered the impact of the uncertainty in the pressure values based on their modelling approach [40]. They found that the PV-based approach (Klotz like) lead to reasonable stiffness results on 18 healthy and pathological cases. We therefore assumed that this approximation can be considered valid for healthy subjects, although probably not for patients. Moreover, our validated models were limited to reflect the mechanical properties of left ventricle in 2-points of the cardiac cycle, end-diastole and end-systole. The unicity of the estimated stiffness and contractility parameters was not mathematically proven. However, by imposing the proportionality between  $b_f$ ,  $b_t$  and  $b_{ft}$  as in [17], the estimation for the passive part is constrained to two parameters only (namely  $C_0$  and  $b_f$ ), enforcing a local convergence to convenient solutions. Furthermore, the co-dependence of the stiffness and contractility parameters is limited by solving sequentially for the two passive parameters ( $C_0$  and  $b_f$ ) and the contractility index ( $CI = T_{max}$ ). Despite remaining issues, the study demonstrates promising value for clinical research as the proposed approach allows the quantification of LV myocardial rigidity and contractility based on a personalized model constructed only from routine cardiac MR data.

### *Conclusion*

Left ventricular stiffness and contractility from 21 normal subjects were estimated using routine cardiac *cine* MR data and personalized cardiac modelling. The modelling approach was extensively validated by comparison of measured/estimated local circumferential strain and other global LV function metrics. The range of biomechanical indices obtained in this study could serve as reference normal values to investigate the degree of severity of ischemic myocardium. The prognosis values of these indices should be explored further within a clinical longitudinal study.

## Appendix A: rule-based myocardial fiber orientation

The rule-based method [16] formulates the spatial distribution of both the helix and the transverse angles based on the local left ventricular coordinates. Within a pseudoprolate LV coordinate system, the local longitudinal coordinate  $u$  is normalized to be  $u = +0.5$  at the basal level and  $u = -1$  at the apex, whereas the radial coordinate is normalized to be  $v = -1$  at the endocardium and  $v = +1$  at the epicardium. The helix angles ( $\alpha_h$ ) and the transverse angles ( $\alpha_t$ ) are described as follows:

$$\alpha_h(u, v) = [h_{10}L_0(v) + h_{11}L_1(v) + h_{12}L_2(v) + h_{13}L_3(v) + h_{14}L_4(v)] \cdot [1 + h_{22}L_2(u) + h_{24}L_4(u)]$$

$$\alpha_t(u, v) = (1 - v^2) \cdot [1 + t_{11}L_1(v) + t_{12}L_2(v)] \cdot [t_{21}L_1(u) + t_{23}L_3(u) + t_{25}L_5(u)]$$

where  $h_{ii}$  and  $t_{ii}$  are scaling parameters for helix and transverse angles, and  $L_i$  are normalized Legendre polynomials of order  $i$ . The scaling parameters are optimized based on [41], and are listed in Table 6.

## Appendix B: myocardial constitutive model

The myocardial mechanical behavior is divided into passive and active parts. The passive part is formulated as a quasi-incompressible transversely-isotropic Fung-type law, originally introduced in [9], whereas the active tension is defined by fiber stretch-dependent active force law [12]. The constitutive laws have been widely used in previous studies [7, 4].

The strain energy density  $W$  is decomposed into two parts: the volumetric part that relates to the change in tissue volume ( $W_V$ ), and the deviatoric part that relates to the change in tissue shape ( $W_I$ ):

$$W = W_V + W_I$$

Table 6: Parameter values for the rule-based myocardial fiber arrangement [41]

Parameters	Values
$h_{10}$	0.362 rad
$h_{11}$	-1.16 rad
$h_{12}$	-0.124 rad
$h_{13}$	0.129 rad
$h_{14}$	-0.0614 rad
$h_{22}$	0.0984
$h_{24}$	-0.0501
$t_{11}$	-0.626
$t_{12}$	0.502
$t_{21}$	0.626 rad
$t_{23}$	0.211 rad
$t_{25}$	0.038 rad

with:

$$W_V = \frac{1}{D} \left( J - \frac{1}{J} \right)$$

where  $D$  determines the material incompressibility and  $J$  is the Jacobian of the deformation gradient  $\mathbf{F}$ :  $J = \det(\mathbf{F})$ . To enforce quasi-incompressibility,  $D$  is set to 0.001 in our study, so that the bulk modulus of the tissue is close to that of water.

The deviatoric part of the strain energy density function is as follows:

$$\begin{aligned} W_I &= \frac{C_0}{2} (e^{\bar{Q}} - 1) \\ \bar{Q} &= b_f \bar{E}_{ff}^2 + b_t (\bar{E}_{ss}^2 + \bar{E}_{nn}^2 + \bar{E}_{sn}^2 + \bar{E}_{ns}^2) \\ &\quad + b_{ft} (\bar{E}_{fs}^2 + \bar{E}_{sf}^2 + \bar{E}_{fn}^2 + \bar{E}_{nf}^2) \end{aligned}$$

where  $C_0$  is the linear passive parameter constant,  $b_f$ ,  $b_t$  and  $b_{ft}$  are the exponential parameter constants. In this study, we kept the exponential ratio fixed, i.e.  $b_f : b_t : b_{ft}$  is equal to 1.0 : 0.4 : 0.7, in accordance to the findings by Wenk et al [17].  $\mathbf{E}$  is the Green-Lagrange strain tensor, where the prefixes  $f$ ,  $s$  and  $n$

denote the myofiber, sheet and sheet-normal directions, respectively.  $\bar{\mathbf{E}}$  is the deviatoric part of the Green strain, which is defined by:

$$\bar{\mathbf{E}} = \frac{1}{2}(\bar{\mathbf{F}}^T \cdot \bar{\mathbf{F}} - \mathbf{I})$$

with  $\bar{\mathbf{F}} = J^{-\frac{1}{3}} \mathbf{F}$

The stiffness index proposed in our study is defined in accordance to the linearization of the stress-strain relationship described in [42] (Chapter 1, equation 23 and 24):

$$E^{(1)} = \frac{C_0}{2}(2b_f + b_t) = \mathbf{SI} \quad (1)$$

$$E^{(2)} = E^{(3)} = \frac{C_0 b_t (2b_f + b_t)}{b_f + b_t} \quad (2)$$

where  $E^{(i)}$  denotes the linearized stiffness in the  $i$  direction. The stiffness index  $\mathbf{SI}$  (Eq. 1) was therefore defined as the amplitude of the initial Young's modulus of the passive myocardium in the fiber direction  $E^f$  (i.e.,  $\mathbf{SI} = E^f = E^{(1)}$ ). Using a transversely-isotropic constitutive law and assuming  $b_t = 0.4b_f$  and  $b_{ft} = 0.7b_f$ , the expressions of the Youngs moduli in the fiber and cross-fiber ( $E^{cf}$ ) directions become:  $E^f = E^{(1)} = 1.2 C_0 b_f$  and  $E^{cf} = E^{(2)} = E^{(3)} = 0.69 C_0 b_f$ .

During active contraction, the active tension is added to the passive second Piola-Kirchhoff stress tensor  $\mathbf{T}$  as follows:

$$\mathbf{T} = \mathbf{T}_{passive} + \mathbf{T}_{active}$$

where  $\mathbf{T}_{passive}$  is the first derivation of the strain energy density function with respect to the Green strain tensor, i.e.  $\frac{\partial W}{\partial \mathbf{E}}$ . The active tension is dependent on the stretch in the local myofiber direction as follows:

$$\mathbf{T}_{active} = T_{max} \frac{Ca_0^2}{Ca_0^2 + ECa_{50}^2} C_t$$

where  $T_{max}$  is the active parameter need to be identified, representing the maximum isometric tension the tissue is able to generate.  $Ca_0$  is the peak intracellular calcium concentration. The length-dependent calcium sensitivity ( $ECa_{50}^2$ ),

the time-related scaling ( $C_t$ ), and the current sarcomere length ( $l$ ) are given by:

$$ECa_{50} = \frac{(Ca_0)_{max}}{\sqrt{e^{B(l-l_0)} - 1}}$$

and

$$C_t = \frac{1}{2}((1 - \cos(\omega)))$$

$$\omega = \begin{cases} 0 \leq t < t_0 & \pi \frac{t}{t_0} \\ t_0 \leq t < (t_0 + t_r) & \pi \frac{t-t_0+t_r}{t_r} \\ (t_0 + t_r) \leq t & 0 \end{cases}$$

$$t_r = ml + b$$

and

$$l = l_r \sqrt{2E_{ff} + 1}$$

where  $(Ca_0)_{max}$  is the maximum peak intracellular calcium concentration,  $B$  is a constant that governs the shape of peak isometric tension-sarcomere length relation,  $l_0$  is the sarcomere length when no active tension develops,  $t_0$  is the peak tension time,  $t_r$  is the duration of the relaxation,  $m$  and  $b$  are constants that govern the relation of the relaxation duration and sarcomere length, and  $l_r$  is the stress-free sarcomere length. The values of the parameters are listed in Table 7 in accordance to [12]. We defined the patient specific contractility index as :  $CI = T_{max}$ .

### Acknowledgements

GK Rumindo was supported by the European Commission H2020 MSCA Training Network VPH-CaSE ([www.vph-case.eu](http://www.vph-case.eu)), grant agreement No 642612. This work was performed within the LABEX PRIMES (ANR-11-LABX-0063) of Université de Lyon, within the program *Investissements d'Avenir* (ANR-11-IDEX-0007) operated by the French National Research Agency.

Table 7: Parameter values of the active tension constitutive law [12]

<b>Parameters</b>	<b>Values</b>
$Ca_0$	$4.35 \mu M$
$(Ca_0)_{max}$	$4.35 \mu M$
$B$	$4.75 / \mu m$
$l_0$	$1.58 \mu m$
$t_0$	$0.1 s$
$m$	$1.0489 s / \mu m$
$b$	$-1.429 s$
$l_r$	$1.85 \mu m$

### Statements

- Conflicts of Interest: None
- Funding: Funding: European Commission H2020 MSCA Training Network VPH-CaSE ([www.vph-case.eu](http://www.vph-case.eu)), grant agreement No 642612.
- Ethical Approval: Not required

### References

- [1] W. J. Richardson, S. A. Clarke, T. A. Quinn, J. W. Holmes, Physiological implications of myocardial scar structure, *Compr Physiol* 5 (4) (2015) 1877–909. doi:10.1002/cphy.c140067.
- [2] V. Y. Wang, P. M. Nielsen, M. P. Nash, Image-based predictive modeling of heart mechanics, *Annu Rev Biomed Eng* 17 (2015) 351–83. doi:10.1146/annurev-bioeng-071114-040609.
- [3] J. Xi, P. Lamata, S. Niederer, S. Land, W. Shi, X. Zhuang, S. Ourselin, S. G. Duckett, A. K. Shetty, C. A. Rinaldi, D. Rueckert, R. Razavi, N. P. Smith, The estimation of patient-specific cardiac diastolic functions from

- clinical measurements, *Medical Image Analysis* 17 (2) (2013) 133–146. doi:10.1016/j.media.2012.08.001.
- [4] V. Y. Wang, H. I. Lam, D. B. Ennis, B. R. Cowan, A. A. Young, M. P. Nash, Modelling passive diastolic mechanics with quantitative MRI of cardiac structure and function, *Medical Image Analysis* 13 (5) (2009) 773–784. doi:10.1016/j.media.2009.07.006.
- [5] J. C. Walker, M. B. Ratcliffe, P. Zhang, A. W. Wallace, B. Fata, E. W. Hsu, D. Saloner, J. M. Guccione, MRI-based finite-element analysis of left ventricular aneurysm, *Am J Physiol Heart Circ Physiol* 289 (2) (2005) H692–700. doi:01226.2004[pii]10.1152/ajpheart.01226.2004.
- [6] H. Gao, A. Aderhold, K. Mangion, X. Luo, D. Husmeier, C. Berry, Changes and classification in myocardial contractile function in the left ventricle following acute myocardial infarction, *J R Soc Interface* 14 (132) (2017). doi:10.1098/rsif.2017.0203.
- [7] M. Genet, L. C. Lee, R. Nguyen, H. Haraldsson, G. Acevedo-Bolton, Z. Zhang, L. Ge, K. Ordovas, S. Kozerke, J. M. Guccione, Distribution of normal human left ventricular myofiber stress at end diastole and end systole: a target for in silico design of heart failure treatments, *J Appl Physiol* 117 (2) (2014) 142–52. doi:10.1152/jappphysiol.00255.2014.
- [8] E. Pena, P. Tracqui, A. Azancot, M. Doblare, J. Ohayon, Unraveling changes in myocardial contractility during human fetal growth: a finite element analysis based on in vivo ultrasound measurements, *Ann Biomed Eng* 38 (8) (2010) 2702–15. doi:10.1007/s10439-010-0010-x.
- [9] J. M. Guccione, A. D. McCulloch, L. K. Waldman, Passive material properties of intact ventricular myocardium determined from a cylindrical model, *J Biomech Eng* 113 (1) (1991) 42–55. doi:10.1115/1.2894084.
- [10] G. A. Holzapfel, R. W. Ogden, Constitutive modelling of passive myocardium: a structurally based framework for material characterization,

- Philos Trans A Math Phys Eng Sci 367 (1902) (2009) 3445–75. doi:10.1098/rsta.2009.0091.
- [11] J. Bestel, F. Clément, M. Sorine, A biomechanical model of muscle contraction, in: W. J. Niessen, M. A. Viergever (Eds.), *Medical Image Computing and Computer-Assisted Intervention MICCAI 2001*, Springer Berlin Heidelberg, 2001, pp. 1159–1161. doi:10.1007/3-540-45468-3\_143.
- [12] J. M. Guccione, L. K. Waldman, A. D. McCulloch, Mechanics of active contraction in cardiac muscle: Part II cylindrical models of the systolic left ventricle, *Journal of Biomechanical Engineering* 115 (1) (1993) 82–90. doi:10.1115/1.2895474.
- [13] C. Tobon-Gomez, M. De Craene, K. McLeod, L. Tautz, W. Shi, A. Hennemuth, A. Prakosa, H. Wang, G. Carr-White, S. Kapetanakis, A. Lutz, V. Rasche, T. Schaeffter, C. Butakoff, O. Friman, T. Mansi, M. Sermesant, X. Zhuang, S. Ourselin, H. O. Peitgen, X. Pennec, R. Razavi, D. Rueckert, A. F. Frangi, K. S. Rhode, Benchmarking framework for myocardial tracking and deformation algorithms: an open access database, *Med Image Anal* 17 (6) (2013) 632–48. doi:10.1016/j.media.2013.03.008.
- [14] L. Asner, M. Hadjicharalambous, R. Chabiniok, D. Peresutti, E. Sammut, J. Wong, G. Carr-White, P. Chowienczyk, J. Lee, A. King, N. Smith, R. Razavi, D. Nordsletten, Estimation of passive and active properties in the human heart using 3D tagged MRI, *Biomechanics and Modeling in Mechanobiology* 15 (5) (2016) 1121–1139. doi:10.1007/s10237-015-0748-z.
- [15] L. Asner, M. Hadjicharalambous, R. Chabiniok, D. Peressutti, E. Sammut, J. Wong, G. Carr-White, R. Razavi, A. P. King, N. Smith, J. Lee, D. Nordsletten, Patient-specific modeling for left ventricular mechanics using data-driven boundary energies, *Computer Methods in Applied Mechanics and Engineering* 314 (2017) 269–295. doi:10.1016/j.cma.2016.08.002.

- [16] P. Bovendeerd, W. Kroon, T. Delhaas, Determinants of left ventricular shear strain, *Am. J. Physiol. Heart Circ. Physiol.* 297 (2009) H1058H1068. doi:10.1152/ajpheart.01334.2008.
- [17] J. F. Wenk, D. Klepach, L. C. Lee, Z. Zhang, L. Ge, E. E. Tseng, A. Martin, S. Kozerke, J. H. Gorman, R. C. Gorman, J. M. Guccione, First evidence of depressed contractility in the border zone of a human myocardial infarction, *The Annals of Thoracic Surgery* 93 (4) (2012) 1188–1193. doi:10.1016/j.athoracsur.2011.12.066.
- [18] G. A. Holzapfel, *Nonlinear Solid Mechanics: A Continuum Approach for Engineering*, Wiley, 2000.
- [19] K. Sun, N. Stander, C. S. Jhun, Z. Zhang, T. Suzuki, G. Y. Wang, M. Saeed, A. W. Wallace, E. E. Tseng, A. J. Baker, D. Saloner, D. R. Einstein, M. B. Ratcliffe, J. M. Guccione, A computationally efficient formal optimization of regional myocardial contractility in a sheep with left ventricular aneurysm, *J Biomech Eng* 131 (11) (2009) 111001. doi:10.1115/1.3148464.
- [20] S. Klotz, I. Hay, M. L. Dickstein, G.-H. Yi, J. Wang, M. S. Maurer, D. A. Kass, D. Burkhoff, Single-beat estimation of end-diastolic pressure-volume relationship: a novel method with potential for noninvasive application, *American Journal of Physiology-Heart and Circulatory Physiology* 291 (1) (2006) H403–H412. doi:10.1152/ajpheart.01240.2005.
- [21] J. C. Lagarias, J. A. Reeds, M. H. Wright, P. E. Wright, Convergence properties of the Nelder–Mead simplex method in low dimensions, *SIAM Journal on Optimization* 9 (1) (1998) 112–147. doi:10.1137/S1052623496303470.
- [22] D. Augustine, A. Lewandowski, M. Lazdam, A. Rai, J. Francis, S. Myerson, A. Noble, H. Becher, S. Neubauer, S. Petersen, P. Leeson, Global and regional left ventricular myocardial deformation measures by magnetic resonance feature tracking in healthy volunteers: comparison with tagging

and relevance of gender, *Journal of Cardiovascular Magnetic Resonance* 15 (1) (2013) 8. doi:10.1186/1532-429X-15-8.

- [23] A. Padiyath, P. Gribben, R. Abraham Joseph, L. Li, S. Rangamani, A. Schuster, A. Danford David, G. Pedrizzetti, S. Kutty, Echocardiography and cardiac magnetic resonance-based feature tracking in the assessment of myocardial mechanics in Tetralogy of Fallot: An intermodality comparison, *Echocardiography* 30 (2) (2012) 203–210. doi:10.1111/echo.12016.
- [24] J. C. Lu, J. A. Connelly, L. Zhao, P. P. Agarwal, A. L. Dorfman, Strain measurement by cardiovascular magnetic resonance in pediatric cancer survivors: validation of feature tracking against harmonic phase imaging, *Pediatric Radiology* 44 (9) (2014) 1070–1076. doi:10.1007/s00247-014-2992-2.
- [25] A. Schuster, G. Morton, S. T. Hussain, R. Jogiya, S. Kutty, K. N. Asrress, M. R. Makowski, B. Bigalke, D. Perera, P. Beerbaum, E. Nagel, The intra-observer reproducibility of cardiovascular magnetic resonance myocardial feature tracking strain assessment is independent of field strength, *Eur J Radiol* 82 (2013). doi:10.1016/j.ejrad.2012.11.012.
- [26] J. Xi, P. Lamata, W. Shi, S. Niederer, S. Land, D. Rueckert, S. G. Duckett, A. K. Shetty, C. A. Rinaldi, R. Razavi, N. Smith, An automatic data assimilation framework for patient-specific myocardial mechanical parameter estimation, in: D. N. Metaxas, L. Axel (Eds.), *Functional Imaging and Modeling of the Heart*, Springer Berlin Heidelberg, 2011, pp. 392–400. doi:10.1007/978-3-642-21028-0\_50.
- [27] A. Nasopoulou, A. Shetty, J. Lee, D. Nordsletten, C. A. Rinaldi, P. Lamata, S. Niederer, Improved identifiability of myocardial material parameters by an energy-based cost function, *Biomechanics and Modeling in Mechanobiology* 16 (3) (2017) 971–988. doi:10.1007/s10237-016-0865-3.
- [28] Z. J. Wang, V. Y. Wang, C. P. Bradley, M. P. Nash, A. A. Young, J. J. Cao, Left ventricular diastolic myocardial stiffness and end-diastolic myofibre

stress in human heart failure using personalised biomechanical analysis, *Journal of Cardiovascular Translational Research* 11 (4) (2018) 346–356. doi:10.1007/s12265-018-9816-y.

- [29] R. M. Lang, M. Bierig, R. B. Devereux, F. A. Flachskampf, E. Foster, P. A. Pellikka, M. H. Picard, M. J. Roman, J. Seward, J. S. Shanewise, S. D. Solomon, K. T. Spencer, M. St John Sutton, W. J. Stewart, Recommendations for chamber quantification: A report from the american society of echocardiography guidelines and standards committee and the chamber quantification writing group, developed in conjunction with the european association of echocardiography, a branch of the european society of cardiology, *Journal of the American Society of Echocardiography* 18 (12) (2005) 1440–1463. doi:10.1016/j.echo.2005.10.005.
- [30] N. Kawel, B. Turkbey Evrim, J. J. Carr, J. Eng, S. Gomes Antoinette, W. G. Hundley, C. Johnson, C. Masri Sofia, R. Prince Martin, J. van der Geest Rob, A. C. Lima Joo, A. Bluemke David, Normal left ventricular myocardial thickness for middle-aged and older subjects with steady-state free precession cardiac magnetic resonance, *Circulation: Cardiovascular Imaging* 5 (4) (2012) 500–508. doi:10.1161/CIRCIMAGING.112.973560.
- [31] J. Ubachs, E. Heiberg, K. Steding, H. Arheden, Normal values for wall thickening by magnetic resonance imaging, *Journal of Cardiovascular Magnetic Resonance* 11 (1) (2009) P61. doi:10.1186/1532-429X-11-S1-P61.
- [32] J. C. L. Rodrigues, S. Rohan, A. G. Dastidar, A. Trickey, G. Szantho, L. E. K. Ratcliffe, A. E. Burchell, E. C. Hart, C. Bucciarelli-Ducci, M. C. K. Hamilton, A. K. Nightingale, J. F. R. Paton, N. E. Manghat, D. H. MacIver, The relationship between left ventricular wall thickness, myocardial shortening, and ejection fraction in hypertensive heart disease: Insights from cardiac magnetic resonance imaging, *The Journal of Clinical Hypertension* 18 (11) (2016) 1119–1127. doi:10.1111/jch.12849.
- [33] K. Mangion, G. Clerfond, C. McComb, D. Carrick, S. M. Rauhalammi,

- J. McClure, D. S. Corcoran, R. Woodward, V. Orchard, A. Radjenovic, X. Zhong, C. Berry, Myocardial strain in healthy adults across a broad age range as revealed by cardiac magnetic resonance imaging at 1.5 and 3.0T: Associations of myocardial strain with myocardial region, age, and sex, *Journal of Magnetic Resonance Imaging* 44 (5) (2016) 1197–1205. doi: 10.1002/jmri.25280.
- [34] S. A. Kleijn, N. G. Pandian, J. D. Thomas, L. Perez de Isla, O. Kamp, M. Zuber, P. Nihoyannopoulos, T. Forster, H.-J. Nesser, A. Geibel, W. Gorissen, J. L. Zamorano, Normal reference values of left ventricular strain using three-dimensional speckle tracking echocardiography: results from a multicentre study, *European Heart Journal - Cardiovascular Imaging* 16 (4) (2014) 410–416. doi:10.1093/ehjci/jeu213.
- [35] K. Kalam, P. Otahal, T. H. Marwick, Prognostic implications of global lv dysfunction: a systematic review and meta-analysis of global longitudinal strain and ejection fraction, *Heart* 100 (21) (2014) 1673. doi:10.1136/heartjnl-2014-305538.
- [36] C. C. Moore, C. H. Lugo-Olivieri, E. R. McVeigh, E. A. Zerhouni, Three-dimensional systolic strain patterns in the normal human left ventricle: characterization with tagged MR imaging, *Radiology* 214 (2) (2000) 453–466. doi:10.1148/radiology.214.2.r00fe17453.
- [37] C. H. Lorenz, J. S. Pastorek, J. M. Bundy, Delineation of normal human left ventricular twist throughout systole by tagged cine magnetic resonance imaging, *J Cardiovas Magn Reson* 2 (2000). doi:10.3109/10976640009148678.
- [38] A. A. Young, H. Imai, C. N. Chang, L. Axel, Two-dimensional left ventricular deformation during systole using magnetic resonance imaging with spatial modulation of magnetization, *Circulation* 89 (1994). doi: 10.1161/01.CIR.89.2.740.

- [39] B. D. Rosen, J. A. C. Lima, The prognostic value of global circumferential strain in patients with suspected myocardial disease, *JACC: Cardiovascular Imaging* 8 (5) (2015) 550. doi:10.1016/j.jcmg.2015.02.008.
- [40] J. Xi, W. Shi, D. Rueckert, R. Razavi, N. P. Smith, P. Lamata, Understanding the need of ventricular pressure for the estimation of diastolic biomarkers, *Biomechanics and Modeling in Mechanobiology* 13 (4) (2014) 747–757. doi:10.1007/s10237-013-0531-y.
- [41] J. Rijcken, P. H. Bovendeerd, A. J. Schoofs, D. H. van Campen, T. Arts, Optimization of cardiac fiber orientation for homogeneous fiber strain during ejection, *Ann Biomed Eng* 27 (3) (1999) 289–97. doi:10.1114/1.147.
- [42] Y. Payan, J. Ohayon, *Biomechanics of Living Organs: Hyperelastic Constitutive Laws for Finite Element Modeling*, Academic Press, 2017. doi:10.1016/C2015-0-00832-2.
- [43] G. Balaban, H. Finsberg, S. Funke, T. F. Hland, E. Hopp, J. Sundnes, S. Wall, M. E. Rognes, In vivo estimation of elastic heterogeneity in an infarcted human heart, *Biomechanics and Modeling in Mechanobiology* 17 (5) (2018) 1317–1329. doi:10.1007/s10237-018-1028-5.
- [44] S. Marchesseau, H. Delingette, M. Sermesant, R. Cabrera-Lozoya, C. Tobon-Gomez, P. Moireau, R. M. Figueras i Ventura, K. Lekadir, A. Hernandez, M. Garreau, E. Donal, C. Leclercq, S. G. Duckett, K. Rhode, C. A. Rinaldi, A. F. Frangi, R. Razavi, D. Chapelle, N. Ayache, Personalization of a cardiac electromechanical model using reduced order unscented kalman filtering from regional volumes, *Med Image Anal* 17 (7) (2013) 816–29. doi:10.1016/j.media.2013.04.012.
- [45] V. Y. Wang, J. A. Niestrawska, A. J. Wilson, G. B. Sands, A. A. Young, I. J. LeGrice, M. P. Nash, Image-driven constitutive modeling of myocardial fibrosis, *International Journal for Computational Methods in Engineering Science and Mechanics* 17 (3) (2016) 211–221. doi:10.1080/15502287.2015.1082675.

- [46] J. D. Bayer, R. C. Blake, G. Plank, N. A. Trayanova, A novel rule-based algorithm for assigning myocardial fiber orientation to computational heart models, *Ann Biomed Eng* 40 (10) (2012) 2243–54. doi:10.1007/s10439-012-0593-5.  
URL <http://www.ncbi.nlm.nih.gov/pubmed/22648575>
- [47] P. M. Nielsen, I. J. Le Grice, B. H. Smaill, P. J. Hunter, Mathematical model of geometry and fibrous structure of the heart, *Am J Physiol* 260 (4 Pt 2) (1991) H1365–78. doi:10.1152/ajpheart.1991.260.4.H1365.
- [48] S. A. Niederer, P. J. Hunter, N. P. Smith, A quantitative analysis of cardiac myocyte relaxation: A simulation study, *Biophysical Journal* 90 (5) (2006) 1697–1722. doi:<https://doi.org/10.1529/biophysj.105.069534>.
- [49] P. J. Hunter, A. D. McCulloch, H. E. ter Keurs, Modelling the mechanical properties of cardiac muscle, *Prog Biophys Mol Biol* 69 (2-3) (1998) 289–331. doi:10.1016/s0079-6107(98)00013-3.